crystals

MDPI

Article

In Situ Synthesis of NPC-Cu_2O/CuO/rGO Composite via Dealloying and Microwave-Assisted Hydrothermal Technique

Mircea Nicolaescu [1], Sebastian Ambrus [2], Petru Hididis [2], Mina Morariu (Popescu) [1,3], Iosif Hulka [4], Corina Orha [1], Carmen Lazau [1], Cosmin Codrean [2,*] and Cornelia Bandas [1,*]

[1] Condensed Matter Department, National Institute for Research and Development in Electrochemistry and Condensed Matter Timisoara, 300224 Timisoara, Romania; mircea.nicolaescu@student.upt.ro (M.N.); mina.popescu@student.upt.ro (M.M.); orha.corina@gmail.com (C.O.); carmen.lazau@gmail.com (C.L.)
[2] Department of Materials and Fabrication Engineering, Politehnica University of Timisoara, 300006 Timisoara, Romania; sebastian.ambrus@upt.ro (S.A.); petru.hididis@student.upt.ro (P.H.)
[3] Department of Applied Chemistry and Engineering of Inorganic Compounds and Environment, Politehnica University of Timisoara, 300223 Timisoara, Romania
[4] Research Institute for Renewable Energies, Politehnica University of Timisoara, 300501 Timisoara, Romania; iosif.hulka@upt.ro
* Correspondence: cosmin.codrean@upt.ro (C.C.); cornelia.bandas@gmail.com (C.B.)

Abstract: The nanoporous copper (NPC)-copper oxides (Cu_2O/CuO)/reduced graphene oxide (rGO) composite structure was synthesized by combining the dealloying process of $Cu_{48}Zr_{47}Al_5$ amorphous ribbons with a microwave-assisted hydrothermal technique at a temperature of 200 °C. The main advantage of the microwave-assisted hydrothermal process is the oxidation of nanoporous copper together with the in situ reduction of graphene oxide to form rGO. The integration of rGO with NPC improves electrical conductivity and streamlines the process of electron transfer. This composite exhibit considerable potential in electrochemical catalysis application, due to the combined catalytic activity of NPC and the chemical reactivity of rGO. Our study relates the transition to n-type rGO in microwave-assisted hydrothermal reactions, and also the development of an electrode material suitable for electrochemical applications based on the p-p-n junction NPC-Cu_2O/CuO/rGO heterostructure. To confirm the formation of the composite structure, structural, morphological, and optical techniques as XRD, SEM/EDX, UV-Vis and Raman spectroscopy were used. The composite's electrochemical properties were measured by EIS and Mott-Schottky analyses, showing a charge transfer resistance (Rp) of 250 Ω and indicating the type of the semiconductor properties. The calculated carrier densities of 4.2×10^{18} cm^{-3} confirms n-type semiconductor characteristic for rGO, and 7.22×10^{18} cm^{-3} for Cu_2O/CuO indicating p-type characteristic.

Keywords: reduced graphene oxide; dealloying; nanoporous copper; microwave-assisted hydrothermal method

check for updates

Citation: Nicolaescu, M.; Ambrus, S.; Hididis, P.; Morariu, M.; Hulka, I.; Orha, C.; Lazau, C.; Codrean, C.; Bandas, C. In Situ Synthesis of NPC-Cu_2O/CuO/rGO Composite via Dealloying and Microwave-Assisted Hydrothermal Technique. *Crystals* **2024**, *14*, 968. https://doi.org/10.3390/cryst14110968

Academic Editor: John Parthenios

Received: 22 October 2024
Revised: 4 November 2024
Accepted: 5 November 2024
Published: 8 November 2024

Copyright: © 2024 by the authors. Licensee MDPI, Basel, Switzerland. This article is an open access article distributed under the terms and conditions of the Creative Commons Attribution (CC BY) license (https://creativecommons.org/licenses/by/4.0/).

1. Introduction

A great interest in the scientific community was gained recently on the topic of nanostructured semiconductors applied in supercapacitors, chemical sensors, lithium-ion batteries, light emitting diodes, and photocatalysts [1]. Metal oxides could be an ideal material to enhance the performance of graphene-based sensors [2], offering multiple benefits, which comprise the ability to expedite the development of a three-dimensional (3D) conductive porous network to enhance the charge transfer pathway and electrical performance, as well as the ability to modify the surface properties of materials. Compared with the expensive noble metal or other metal oxide nanoparticles, CuO is a cheap alternative with a broad potential application. Copper (Cu) and copper oxide (Cu_2O) nanoparticles are readily available and have attracted considerable attention because they are one of the most important in modern technologies. There is increasing interest in copper nanoparticles due

to their optical, catalytic, mechanical, and electrical properties [3]. Copper oxide shows two oxidation states, namely, cuprous oxide (Cu^{2+}) and cupric oxide (Cu^{+}) [4]. Different CuO morphologies, known as p-type semiconductors [5], have been tested as sensors, i.e., urchins [6], spherically arranged nano-bricks [7], nanoseeds [8], microspheres [9], cotton flower-like [10], nanoparticles [11], faceted, and non-faceted nanoribbons [12]. In the case of graphene-copper oxide (CuO and Cu_2O) composites, the morphology of the copper oxide plays an important role in the functionalization of the composite material. Various copper oxide morphologies wrapped in graphene based material, such as nanocubes [13], porous nano-spheres [14], microspheres [15], hollow cubes [16], nanoparticles [17–19] and so on [20], have been reported in the literature due to their ability to enhance critical characteristics. Different chemical synthesis techniques were followed to develop hybrid materials based on metal oxide and graphite oxide, such as self-assembly, solvothermal, solution mixing method, combustion method, hydrothermal, microwave irradiation, CVD and sol–gel methods [21]. Among these methods, the hydrothermal in the microwave field method is a simple, fast, and environmentally friendly route to obtain hybrid materials.

Graphene has garnered significant attention from researchers because the major drawback of using pristine metal oxide is agglomeration and chemical stabilization, enhancing physical properties [22]. Furthermore, 2D-graphene materials offer interesting electronic, thermal, and mechanical properties and have a large surface area with various functional groups, which provides for chemical modifications, making it an important candidate in many studies (energy storage [23], field effect transistors [24], water desalination [25], gas purification [26], supercapacitors [27], molecular sieving [28], sensors [29], and nucleic acid sequencing [30]).

Recently, various synthesis procedures have been used to obtain Cu_2O and graphene/carbon nanocomposites, such as ultrasonication reduction of graphene oxide (GO) in the Cu_2O precursor solution [31], a layer deposition on Cu_2O by immersion of anodized copper foil in GO solution [32] or by immersion of Cu foil in a glucose solution obtaining a thin carbon layer on Cu_2O nanowires [33]. Recently, Zhao et al. has synthesized CuO–graphene nanostructures using a hydrothermal method in the presence of ammonia solution for use in supercapacitors [34]. Chen et al. described a strategy for the synthesis of nanoporous graphene/Cu_2O composite materials by combustion of graphene oxide and copper chloride in an oven at 450 °C for only one minute. Furthermore, the nanocomposite was used as a new chemiluminescence sensing strategy to determine the nicotinamide adenine dinucleotide in a buffer solution and complex biological matrix with a detection limit of 3.5 nM [35]. Tian et al. successfully synthesized three-dimensional NP-Cu with rich porosity by using a one-step approach to combine controlled alloy refining and facile chemical dealloying. The resulting NP-Cu shows a bicontinuous nanoporous structure with ligaments of ~20 nm. Due to the intrinsic superior electrocatalytic activity of NP-Cu, the team developed an electrochemical sensor based on the composite of NP-Cu and the functionalized RGO for the sensitive determination of carbendazim [36]. The conductivity type of rGO depends on the synthesis conditions, while it is typically a p-type semiconductor, over the years different researchers have synthesized n-type rGO by doping procedures [37], controlling the synthesis temperature range [38,39], by laser irradiation [40], or employing hydrothermal methods [41]. Ma et al. reported a one-step hydrothermal method to prepare a p-n heterojunction of 3D rGO/In_2O_3 nanocomposites with excellent gas sensing properties, gaining a good sensitivity (9.3% at room temperature) for 100 ppm of trimethylamine [42]. Seo Yun Park et al. obtained a fast-responding humidity sensor, a p-n junction between rGO and MoS_2, synthesized through a hydrothermal method. The authors obtained a good response to various gasses such as 10 ppm NO_2, 1000 ppm NH_3, 50 ppm H_2, and 50 ppm C_2H_5OH that was four times higher compared to pristine rGO [43]. Zhang et al. prepared a n–p heterojunction of SnO_2–rGO hybrid composite by a facile hydrothermal synthesis and constructed a ppm-level NO_2 gas sensor on a PCB substrate using a low-cost fabrication method. They obtained a rapid response

and good repeatability at room temperature by exposing the hybrid composite to a wide concentration ranging from 1 to 2000 ppm toward NO_2 gas [44].

Copper primarily exhibits two oxidation states, $^{+}1$ and $^{+}2$, which can be achieved by various oxidation methods, including thermal and chemical processes. Recently, hydrothermal oxidation (HTO) has emerged as an advanced and environmentally friendly approach for material synthesis, offering efficient and sustainable solutions for copper oxidation [45]. Depending on the oxidation process parameters, both CuO and Cu_2O semiconductors can be synthesized with different morphologies. Numerous studies demonstrate that Cu_2O/CuO composites exhibit superior chemical and electrochemical performance across various applications. This enhanced functionality is primarily attributed to the mixed-valence Cu^{+}/Cu^{2+} system, which accelerates certain redox reactions [46]. D. S. Zimbovskii and A. N. Baranov conducted a study on the nucleation and growth of a copper oxide layer during hydrothermal treatment, using metallic copper as a precursor and an alkaline solution for reduction, to synthesize only Cu_2O semiconductor. They demonstrate that alkaline concentration and the amount of oxygen in the system are key parameters influencing the formation of Cu_2O. Furthermore, they present the thermodynamic principles governing the formation of Cu_2O and CuO, detailing the synthesis mechanism involved [47]. The use of Cu_2O/CuO-carbon-based composites provides notable benefits in improving electrochemical and photocatalytic performance. Carbon materials, especially graphene oxide, enhance electron transport, which improves charge separation and allows for better light absorption. This results in higher photocatalytic activity because the electrons in graphene oxide play an active role in optical reactions, leading to better adsorption of pollutants and light absorption compared to pure metal oxides. Moreover, incorporating Cu_2O and CuO in multicomponent systems further enhances efficiency because graphene helps prevent particle aggregation and promotes rapid ion diffusion and electron mobility, ultimately leading to greater stability and durability in energy storage and environmental applications [48,49]. Although the hydrothermal method has been intensively studied for the synthesis of various composite structures based on CuO and Cu_2O, our study focuses on obtaining an NPC-Cu_2O/CuO/rGO composite structure by the microwave-assisted hydrothermal method, a simple and low-cost process in which nanoporous metallic copper was oxidized in situ together with the reduction of graphene oxide. The microwave-assisted hydrothermal method has recently been proven to be an effective technique for producing pure rGO without using of any reducing agents [50]. The mechanism of doped-rGO formation through the hydrothermal method has been explained by Liguo et al., showing that this reduction process involves the removal of small oxygen-containing molecules, such as H_2O and CO, or the removal of NH_2 groups [41]. D. Muthu Gnana Theresa Nathan et al. prepared copper oxides/reduced graphene oxide (Cu_2O-CuO/rGO) nanocomposites with the hydrothermal method. Electrochemical measurements of the nanocomposite demonstrated a high specific capacitance of 436.6 F g^{-1} at 1 A g^{-1} and excellent cyclic stability even after 1000 cycles [48]. Zhao et al. developed an electrode with structures CuO/rGO, rGO/Cu_2O and Cu_2O/Cu by deposition in situ on copper foil using the hydrothermal method. The electrodes were used for achieved a sensor for amperometry detection of glucose and hydrogen peroxide [51]. Wang et al. achieved an nanocomposite based on Cu_2O/CuO/rGO structure by hydrothermal method, and the good electrochemical performance can recommend this nanocomposite material for supercapacitors application, especially due to the fact that the capacitance remained at 98.2% of the initial specific capacitance after 100,000 cycles at 10 Ag^{-1} [52].

To the best of our knowledge, there are no reported works on the in situ synthesis of NPC-Cu_2O/CuO/rGO composite structures in microwave-assisted hydrothermal conditions, the novelty aspects being related to the transition to n-type rGO in microwave-assisted hydrothermal reaction and the development of an electrode material suitable for electrochemical applications based on p-p-n NPC-Cu_2O/CuO/rGO heterostructure junction.

2. Materials and Methods

2.1. Chemicals

Graphene oxide (4 mg mL^{-1}) dispersed in H_2O, hydrofluoric acid (HF) solution (1.5 M), copper (Cu), zirconium (Zr) and aluminum (Al) powders, were purchased from Sigma-Aldrich Company (St. Louis, MO, USA). All reagents were of pure analytical grade and were used without purification.

2.2. Synthesis of the NPC-Cu_2O/CuO/rGO Composite Structure

Obtaining of the NPC-Cu_2O/CuO/rGO composite structures involve using both the dealloying process and the microwave-assisted hydrothermal process, the experimental protocol being presented below:

2.2.1. Synthesis of Amorphous $Cu_{48}Zr_{47}Al_5$

Amorphous ribbon with a nominal composition of $Cu_{48}Zr_{47}Al_5$ was produced by electric arc melting of high-purity (99.9%) materials such as copper (Cu), zirconium (Zr) and aluminum (Al) in a 99% Argon atmosphere. The amorphous structure of the ribbons with a thickness of 20 μm and a width of 2 mm, was produced by melting the alloy by induction process and afterward rapidly supercooled on a copper roll using the "melt spinning" method.

2.2.2. Synthesis of Amorphous NPC

Nanoporous copper (NPC) was obtained by dealloying amorphous ribbons from the $Cu_{48}Zr_{47}Al_5$ alloy. The dealloying process presumes immersion of 0.1 g amorphous ribbons into 10 mL of 1.5 M HF aqueous solution at room temperature for 60 min. To remove any residual HF solution at the end, the materials were rigorously washed with distilled water several times. The as-synthesized NPC was kept in a distilled water suspension at room temperature to avoid natural oxidation.

2.2.3. Preparation of NPC-Cu_2O/CuO/rGO Composite Structure

To study the influence of graphene oxide contents on the formation of NPC-Cu_2O/CuO/rGO composites, a number of samples were obtained by microwave-assisted hydrothermal method using 1.5, 2, 2.5, and 3 mL of GO solution and labeled as NPC-$rGO_{1.5}$, NPC-rGO_2, NPC-$rGO_{2.5}$, and NPC-rGO_3, respectively. Before treatment, the GO solutions were stirred and ultrasound for 2 hours at room temperature for a good dispersion. The GO and NPC were hydrothermally reacted in a Teflon autoclave with a degree of fullness of 10%, placed in a microwave oven at a heating temperature of 200 ° C for 60 min (with a 15 min gradient temperature increase), with the oven power set to 1000 W (Anton Paar, Multiwave 3000 Microwave Digestion Oven, Graz, Austria). Finally, after the process was completed, the autoclaves were cooled to room temperature and the as-obtained NPC-Cu_2O/CuO/rGO composite solutions were stored. The advantage of this process is the oxidation of nanoporous copper at the same time as the in situ reduction of GO to form rGO. The advantages of the microwave-assisted hydrothermal method are related to several aspects, as microwave energy accelerates the processes ensuring higher efficiency, time saving, and precise temperature control [53].

2.3. Materials Characterization

The crystallinity of the composite materials was assessed by X-ray diffraction technique (XRD, PANalytical X'Pert PRO MPD Diffractometer, The Netherlands) with Cu-K radiation in the range 2*theta* = 20–80°. The microstructure of the samples was analyzed by Scanning electron microscopy (SEM, Quanta FEG 250, FEI, Hillsboro, OR, USA) using secondary electron detector (SE) and the elemental analysis was performed by energy dispersive X-ray spectroscopy (EDX with Apolo SSD: detector, EDX with Apolo SSD: detector, EDAX Inc., Mahwah, NJ, USA), was used to evaluate the morphology and purity of the materials. A UV-VIS spectrophotometer (PerkinElmer Lambda 950 UV/Vis, Shelton, WA, USA) with

a 150 mm integrating sphere in the range of 400–900 nm was used to record the optical characteristics. In order to identify the vibrational states of the as-synthesized structures, Raman spectroscopy was used with a Nanonics Imaging (Jerusalem, Israel)—MultiProbe Imaging—MultiView 1000™Platform (SPM) equipped with a 532 nm laser.

2.4. Electrochemical Measurements

Electrochemical experiments were conducted using a classical three-electrode system in a 1 M KOH electrolyte solution, using a potentiostat/galvanostat, PGSTAT 302 from Metrohm Autolab B.V., controlled by Nova 2.1.2 software. The NPC-Cu_2O/CuO/rGO composite samples were deposited on conductive glass with a 0.28 cm^2 area, serving as working electrodes. An Ag/AgCl (saturated KCl) electrode was used as the reference electrode, and a platinum electrode served as the counter electrode.

3. Results and Discussion

The synthesis process and strategy of NPC-Cu_2O/CuO/rGO composite structure are illustrated in Figure 1. The process consists of two stages. In the first stage, the amorphous $Cu_{48}Zr_{47}Al_5$ ribbons were manufactured using the melt spinning method, the dealloying process consisting of immersing 0.1 g amorphous ribbons in 1.5 M HF solution to form nanoporous copper. In the second stage, NPC-Cu_2O/CuO/rGO composite was synthesized in situ via microwave-assisted hydrothermal treatment. The GO and NPC solutions were reacted in a Teflon autoclave at 200 °C for 60 min by microwave-assisted hydrothermal reaction in which the nanoporous copper was in situ oxidized together with the obtaining of n-type rGO forming the NPC-Cu_2O/CuO/rGO p-p-n junction.

The as-obtained composite structures were structurally characterized by XRD analysis, the results are presented in Figure 2. The XRD diffraction patterns of the as-spun ribbons presented in Figure 2a exhibit a broad intensity peak at *2theta* = 35–45°, indicating the amorphous state of the $Cu_{48}Zr_{47}Al_5$ alloy. After dealloying in a 1.5 M HF solution, the diffraction peaks corresponding to metallic copper (111), (200), and (220) with a cubic structure JCPDS No. 00-003-1015 were observed. Furthermore, slight oxidation of copper occurred during the dealloying process, as indicated by the presence of the (111) plane of Cu_2O. Figure 2b shows the X-ray patterns for the as-obtained NPC-Cu_2O/CuO/rGO composite structures indicating the presence of a cubic structure Cu (JCPDS No. 00-003-1015), monoclinic CuO (JCPDS No. 01-074-1021), and a cubic structure Cu_2O (JCPDS No. 01-074-1230). In particular, the presence of rGO peak in NPC-Cu_2O/CuO/rGO composite structures is confirmed by the slight peak at *2theta* = 26°, proving the reduction of graphene oxide, this finding also being confirmed by other studies [54] (Figure 2c). All samples exhibited diffraction peaks near 43.5°, 50.4°, and 74°, corresponding to the (111), (200), and (220) planes of metallic copper from the initial precursor of nanoporous copper, in accordance with our previous study about the synthesis of NPC materials [55]. Due to the oxidation process within the microwave-assisted hydrothermal reaction, the diffraction peaks at *2theta* about 29.6°, 36.6°, 42.5°, 61.6°, 73.9°, and 77.7° are assigned to the (110), (111), (200), (220), (311), and (222) crystal planes of Cu_2O (cuprite). According to the results obtained by D. Ursu et al. [56] which synthesized copper oxides using a metallic precursor within the classical hydrothermal process, together with Cu and Cu_2O some diffraction peaks at 35.7°, 38.9°, 49.0°, 58.6°, 66.1°, and 68.3° assigned to (002), (111), (-202), (202), (022), and (113) plans belong to monoclinic CuO, the most intense peak being observed for the NPC-rGO_3 sample. In another study, Zhang et al. [57] demonstrated that during the classical hydrothermal process, most of the Cu^{2+} ions were reduced to Cu_2O, but in our case the lack of use of reduction agents together with the microwave-assisted hydrothermal process and a large surface area of NPC probably facilitated the formation of heterostructure by oxidation of Cu_2O to CuO.

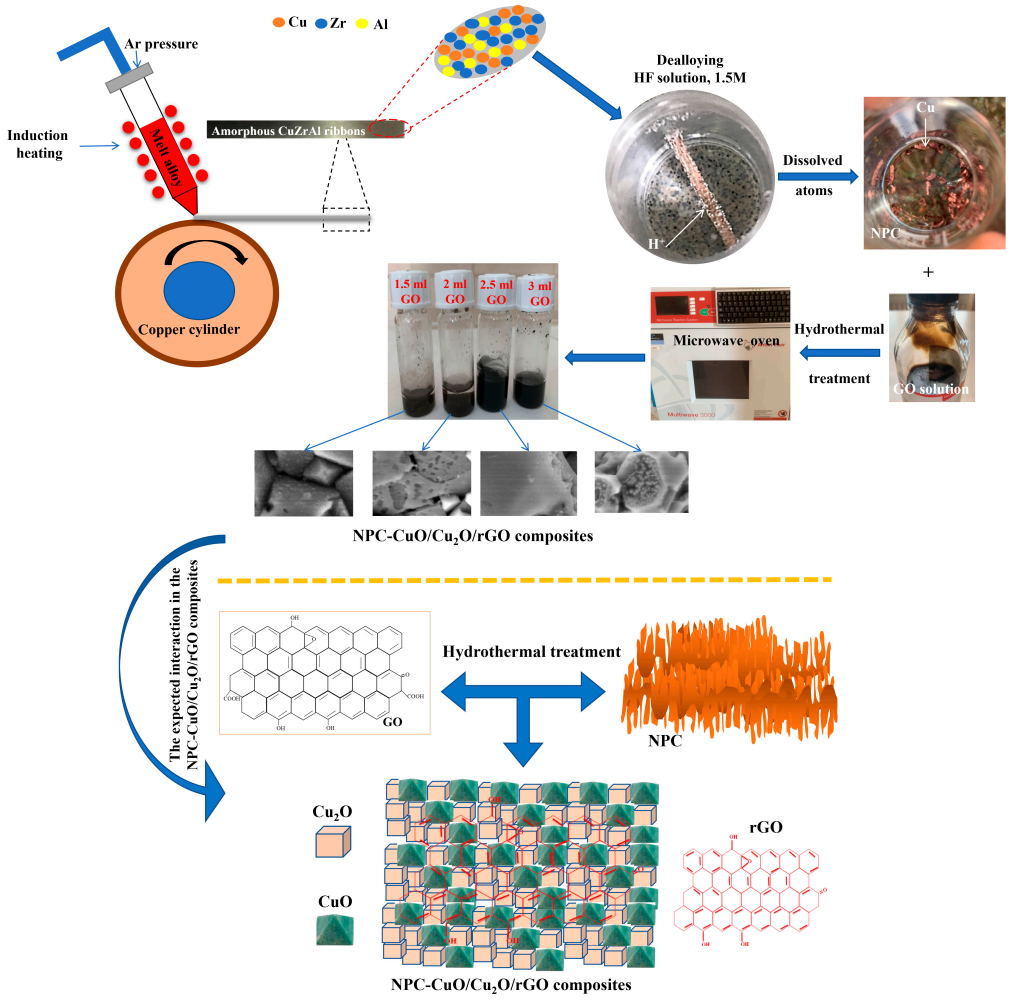
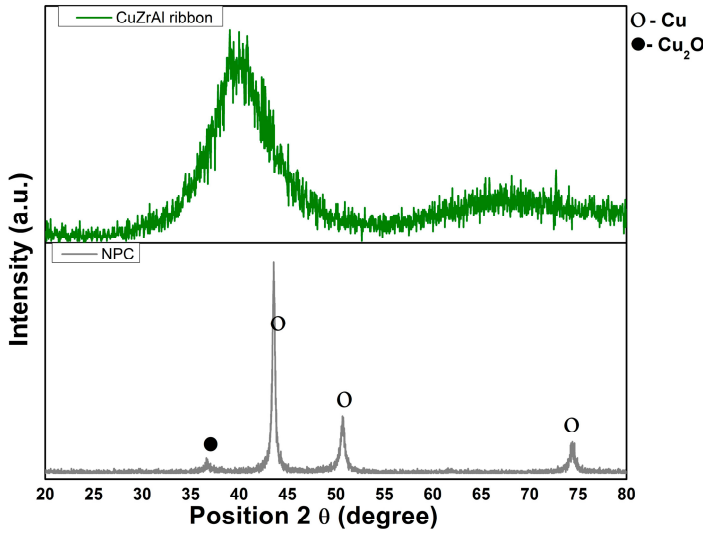


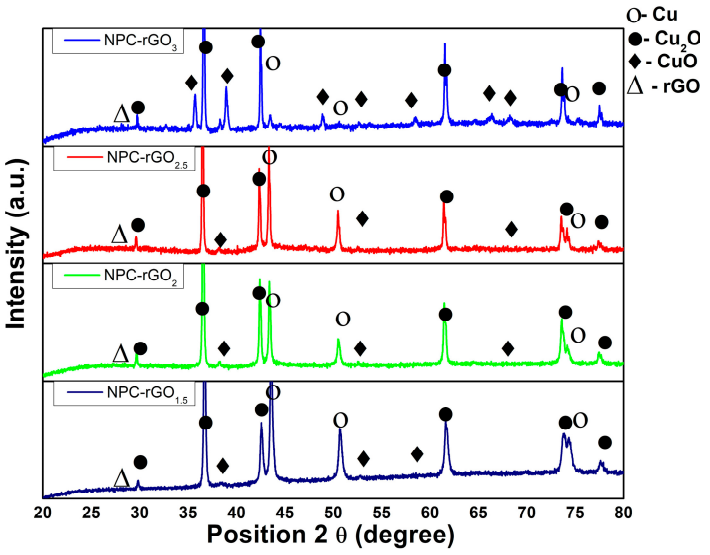
Figure 1. Schematic illustration for the synthesis of NPC-Cu_2O/CuO/rGO composites.

The SEM technique was used to characterize the morphology of the as-synthesized structures. The morphology of the dealloyed copper-based amorphous ribbons in an acidic solution (Figure 3a) and the surface morphology of the synthesized NPC-Cu_2O/CuO/rGO composites (Figure 3b–d) are presented. Additionally, the EDX elemental analysis was performed to confirm the dealloying process and composite synthesis (Figure 3e). Thus, Figure 3a shows that the NPC sample formed from $Cu_{48}Zr_{47}Al_5$ alloy by the dealloying process exhibits a bi-continuous nanoporous structure composed of irregular ligaments, and in some areas, it forms large channels with an average ligament length of 29.31 nm (the pore size was measured using ImageJ software (Version 1.53t) and defined as the distance between the ligaments/particles). For NPC-Cu_2O/CuO/rGO composites, an obvious change in the surface morphology can be observed depending on the experimental parameters. At a lower magnification, it can be seen that the structure of separate islands with larger size was obtained for NPC-$rGO_{1.5}$ and NPC-rGO_2. This phenomenon is probably due to the fact that the volume of graphene in water suspension from the autoclave was varied, thus at a higher solution volume, a higher pressure was generated in the autoclave, which together with the microwave-induced cavitation phenomenon can cause breakage pieces of NPCs at a higher rate when increasing the volume of the graphene oxide solution. Furthermore, on the surface of the islands, different copper oxide morphologies can be observed due to the experimental conditions, with an rGO layer that is more prominent at higher graphene oxide content, appearing as a black shadow covering the metal/oxide composite. The cubic copper oxide can be observed for sample NPC-$rGO_{1.5}$, as shown in Figure 3b, according to XRD analysis. Increasing the content of the graphene oxide solution

to 2 mL (Figure 3c) results in a mixed copper oxide phase with a higher content of monoclinic CuO forming on the Cu_2O crystals. In addition, an overall more porous morphology can be observed. The increase in monoclinic CuO content continues for the NPC-$rGO_{2.5}$ sample in Figure 3d, where some incompletely formed octahedral crystals can be seen in elongated shapes. Instead, a more pronounced octahedral structure of the copper oxide can be observed for the NPC-rGO_3 sample (Figure 3e). At higher magnification, it is evident that these octahedral are made up of smaller nanoparticles assembled in this configuration. In addition, a possible core–shell structure consisting of a copper core and copper oxide nanoparticles can be identified. From the elemental analysis of the EDX spectra (Figure 3f) it was observed that the Al and Zr elements of the precursor alloy are completely removed following the dealloying process. Therefore, all as-synthesized samples presented only Cu, O and C elements attributed to Cu_2O, CuO, and rGO structures, certifying the purity of the structures.

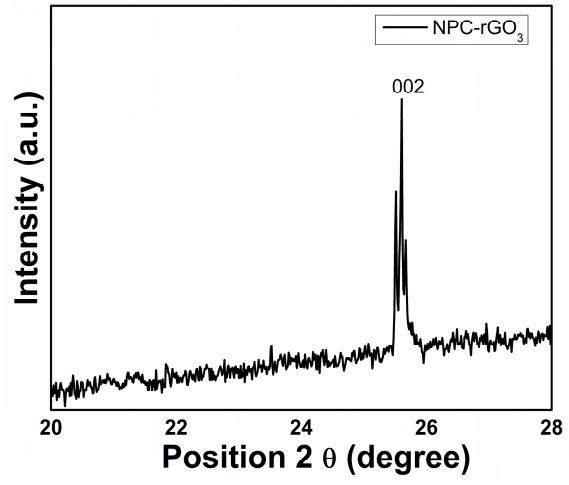


(**a**)



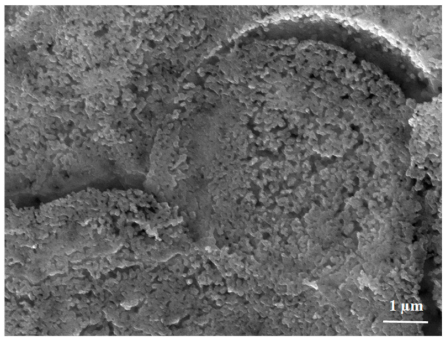
(**b**)

Figure 2. *Cont.*

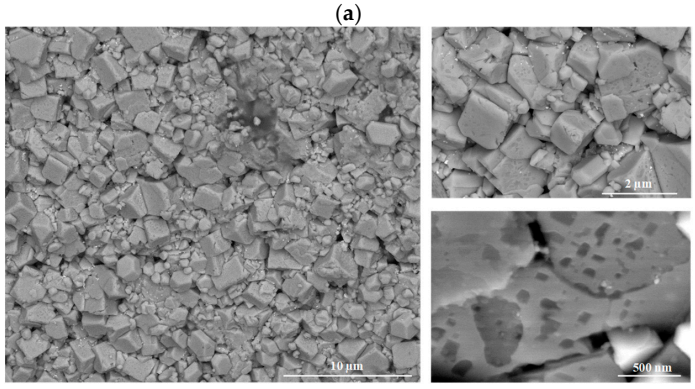


(**c**)

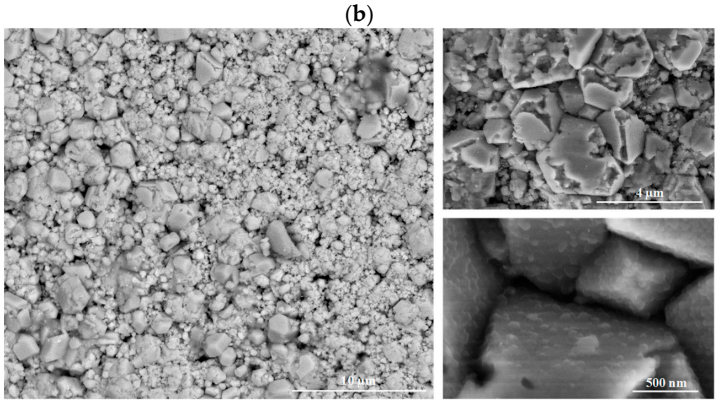
Figure 2. X-ray patterns for as-spun ribbon (**a**); as-obtained NPC-Cu_2O/CuO/rGO composites (**b**) and rGO peak for *2theta* = 20–28° (**c**).



(**a**)



(**b**)



(**c**)

Figure 3. *Cont.*

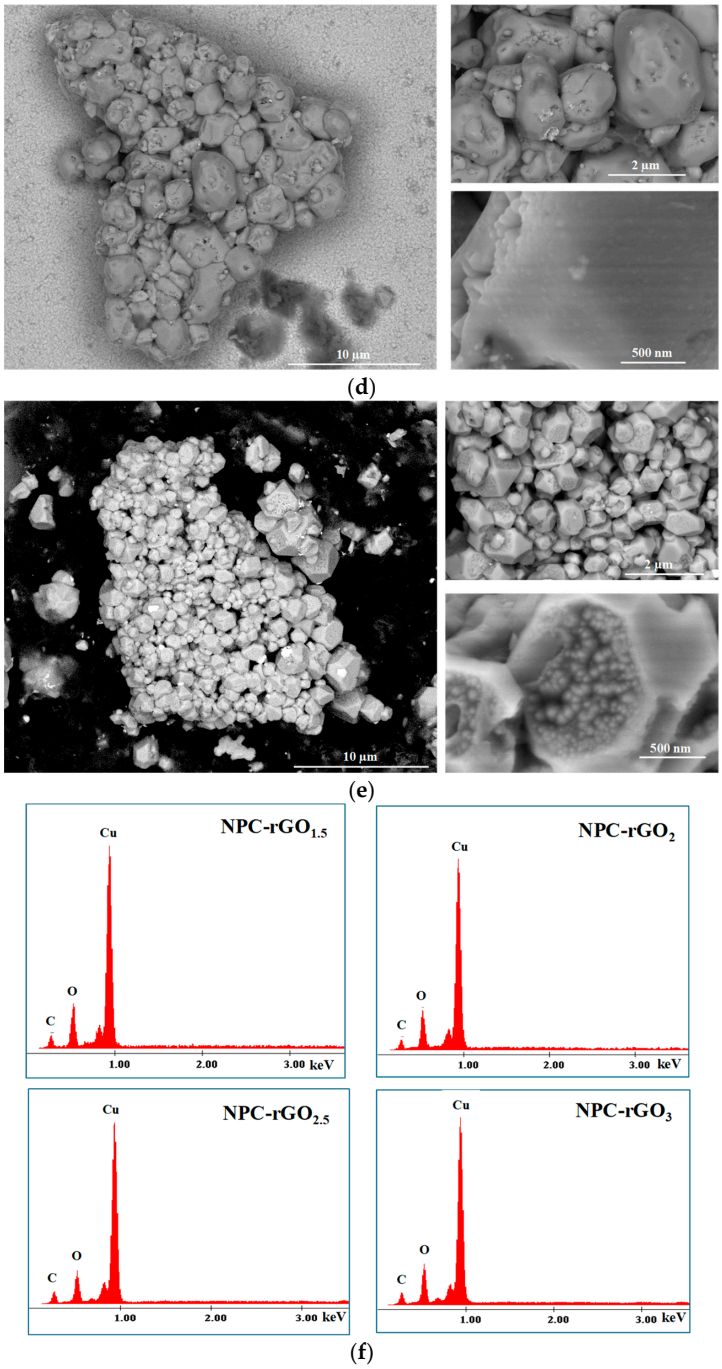


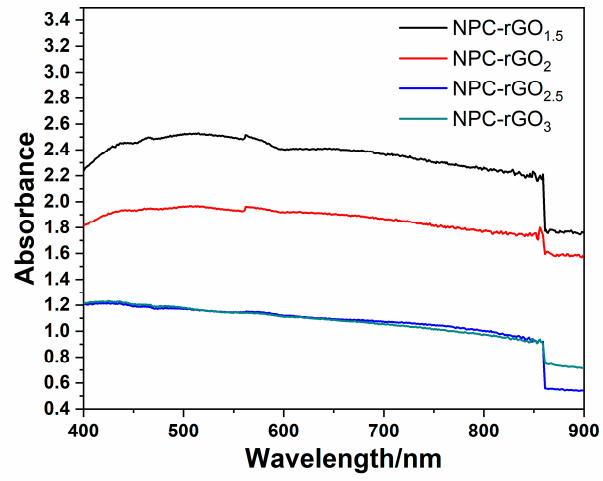
Figure 3. SEM morphologies of the samples NPC (**a**); NPC-rGO$_{1.5}$ (**b**); NPC-rGO$_2$ (**c**); NPC-rGO$_{2.5}$ (**d**) and NPC-rGO$_3$ (**e**). EDX spectra of the as-synthesized samples (**f**).

The optical properties of the structures were evaluated based on a UV-Vis analysis (Figure 4a), and it is evident that the NPC-Cu_2O/CuO/rGO heterojunctions exhibit consistent light absorption, with a slight increase observed in the UV and near-UV spectra. This phenomenon suggests a strong interfacial interaction between rGO and Cu_2O/CuO, which extends the absorption range into the visible-light spectrum [58,59]. The calculated energy bandgap of the as-obtained structures was determined using the Tauc formula, as shown in Figure 4b. The bandgap energy (Eg) was evaluated from the UV-Vis absorption results using Equation (1) [1]:

$$Eg = 1240/\lambda \quad (1)$$

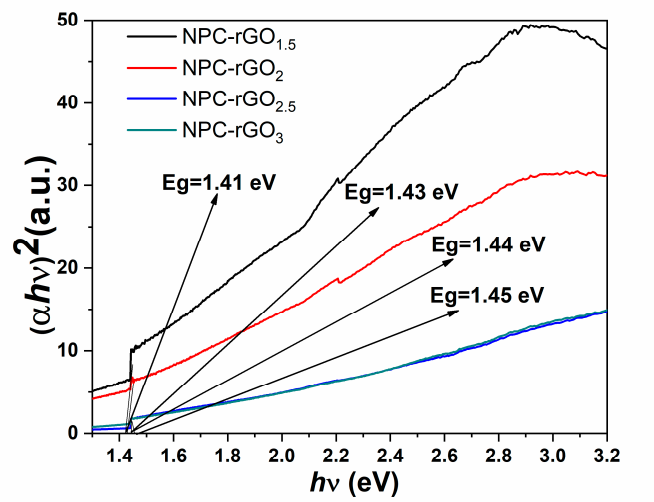
where λ—optical absorption (nm). The bandgaps of the NPC-Cu_2O/CuO/rGO heterojunction around 1.4 eV, with slight variations depending on the experimental conditions compared to the bandgaps of free Cu_2O (2.15 eV) and CuO (1.7 eV) suggest that the hybridization of Cu_2O and CuO forms an alignment of energy levels, which leads to charge redistribution at the interface, and which lowers the Fermi level. This phenomenon enhances the electronic transfer across phase interfaces, as reported in the literature [60,61]. Raman spectroscopy is one of the most effective methods for investigating the ordered and disordered crystal structures of carbon—the spectra from 1000 to 2500 cm^{-1} are presented in Figure 4c. Two distinct peaks, referred to as the G and D bands, are the significant vibrational modes in the Raman spectra of the graphitic structures [1]. As shown, the specific peaks are presented, one about 1350 cm^{-1} attributed to the D band arises from the defect's presence in the hexagonal structure, and another around 1550 cm^{-1} attributed to the G band corresponds to the C-C bonds. In the Raman spectra of bare GO, the ratio I_D/I_G was about 0.85 while for NPC-Cu_2O/CuO/rGO the value increases to 1.10, indicating the appearance of defects after the reduction process and the successful removal of functional oxygen groups [62].Therefore, as presented in Figure 4c the intensities of specific peaks for G and D bands are direct proportional with the amount of GO used in the synthesis of the composite.

For the electrochemical characterization of the NPC-Cu_2O/CuO/rGO composite, the NPC-rGO_3 sample was chosen due to its higher graphene oxide content, which ensures a more conclusive visualization of junction behavior. Electrochemical impedance spectroscopy (EIS) was recorded in the frequency range of 0.1–1000 Hz by applying an AC voltage with a 10 mV amplitude modulation. The Nyquist plot presented in Figure 5 displays three distinct regions, corresponding to different frequency ranges, and by using the equivalent circuit (Inset of Figure 5) the electrochemical data were extracted. The series resistance (Rs) was measured at 40 Ω, which represents the electrolyte resistance between the working and reference electrodes. The charge transfer resistance (Rp) measured at 250 Ω reflects the resistance encountered during the charge transfer process of the as-synthesized NPC-Cu_2O/CuO/rGO composite. The relatively high value of charge transfer resistance observed for the as-obtained composite structure is likely attributed to the poor conductivity of copper oxides [63].

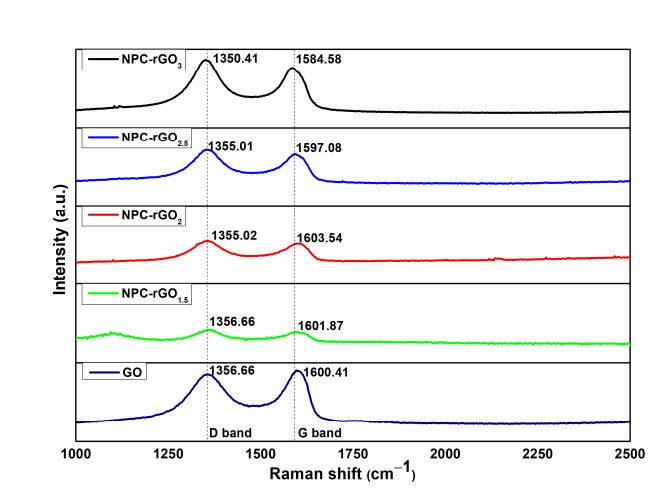


(**a**)

Figure 4. *Cont.*



(**b**)



(**c**)

Figure 4. UV-Vis absorption spectra of the as-obtained structures (**a**); Tauc's plot for *Eg* calculation for structure (**b**); Raman spectra of the composites (**c**).

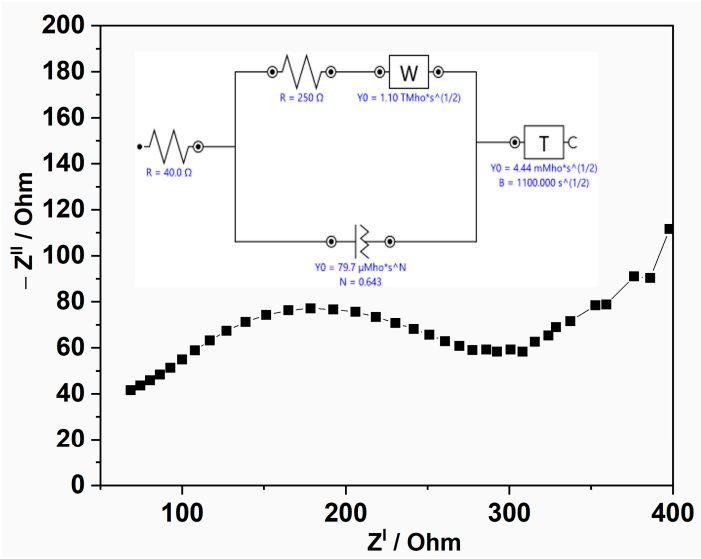


Figure 5. Nyquist plot and equivalent circuit fitting (inset) of the NPC-rGO$_3$ composite.

To evidence the type of semiconductor, the flat band potential, and the carrier density of the as-selected NPC-rGO_3 structure, Mott–Schottky (M–S) measurements were recorded (Figure 6) [64]. M–S measurements were performed between −0.5 V and +2 V at a constant frequency of 1000 Hz.

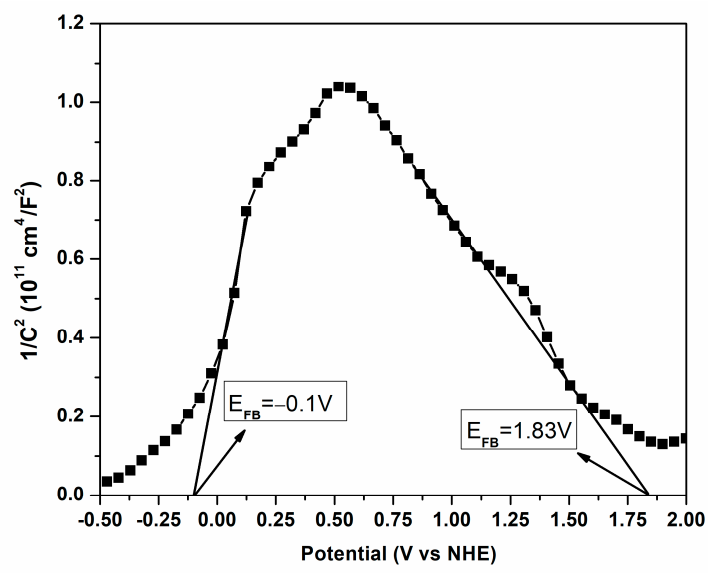


Figure 6. Mott–Schottky analysis of the NPC-rGO_3 composite in 1 M KOH supporting electrolyte.

The energy band diagram of the NPC-rGO_3 was examined using the Mott–Schottky plot based on Equation (2) [65]:

$$\frac{1}{C^2} = \pm \frac{2}{\varepsilon \varepsilon_0 A^2 e N_C} \left(V - V_{FB} - \frac{K_B T}{e} \right) \quad (2)$$

where **C**—represents the capacitance of the semiconductor, $\mathbf{N_c}$—the carrier density (or concentration), ε—the dielectric constant of the semiconductor (for Cu_2O/CuO is 8.93 and 3.50 for rGO), ε_0—the vacuum permittivity (8.854×10^{-14} F cm^{-1}), *e*—the charge of electron, $\mathbf{K_B}$ = 1.381×10^{-23} Boltzmann constant, **A**—the active surface area of the photoelectrode (0.28 cm^2), **T** = 298.15 K the room temperature, **V**—the applied potential and $\mathbf{V_{FB}}$—the flat band potential [5,40,66]. Mott–Schottky analysis was used to determine the flat band potential (V_{FB}) which allows to identify of donor or acceptor density for Cu_2O/CuO and rGO. After extrapolating the linear part of the curve when $1/C2 = 0$, the value of V_{FB} was determined about 0.1 V for rGO and 1.83 V for Cu_2O/CuO vs NHE, where E(NHE) = E (Ag/AgCl) + 0.197 V. The calculated carrier densities are 4.2×10^{18} cm^{-3} for rGO, which registers a positive slope as shown in Figure 6, indicating that it exhibits n-type semiconductor characteristics with a conduction band value of −0.09 V. For Cu_2O/CuO, the carrier density is 7.22×10^{18} cm^{-3} with a valence band value of 1.847 V exhibiting a negative slope and indicating p-type semiconductor characteristics [67].

Researchers have spent a considerable effort over the past few years in developing different structures for electrode materials based on Cu-rGO materials. Within our research, using the microwave-assisted hydrothermal method for the synthesis of NPC-Cu_2O/CuO/rGO composite structure offers many advantages, such as higher efficiency, time saving, precise temperature control, environmentally friendly agents, low production cost, and no use of hazardous chemicals. Table 1 highlights different composite structures obtained by various methods for electrochemical application.

Table 1. Different structures of the electrode materials based on composite materials used in different application fields.

Materials	Electrode Type	Synthesis Method	Application Field	Semiconductor Type	References
3D nanoporous copper/reduced graphene oxide (NP-Cu/RGO)	Electrode sensor (based on glassy electrode modified with the composite NP-Cu and reduced graphene oxide	Melt spinning method	Sensor development/detection	-	[36]
Reduced graphene oxide/porous hollow copper cobalt selenide (rGO-CCSe)	Electrodes	Self-templated method	Hybrid supercapacitors used in modern electronic device	-	[68]
Copper oxide nanoparticles/reduced graphene oxide/pencil graphite electrode (CuO (NP)/ rGO-PGE	Sensor (non-enzymatic glucose sensor)	Dip-coating method	To determine the glucose concentration in human blood serum	-	[69]
Copper oxide/silver/reduced graphene (CuO/Ag/rGO)	Composite electrode materials	Hydrothermal method	Supercapacitors	-	[70]
Nanoporous copper/copper oxide composite (NPC/Cu_2O)	Composite electrode	Dealloying process	Capacitors	-	[71]
Reduced graphene oxide thin films (rGO)	Material (Conversion of p to n)	Pulsed Laser annealing	-	n-type	[40]
Copper oxide hetereostructures (Cu_2O/CuO)	Heterostructure photocathode	Thermal annealing	Photoelectrochemical water splitting	p-type	[5]
Copper oxides/anchored reduced graphene nanosheets (CuO-Cu_2O@ rGO NPC)	Nanocomposite electrode	Seed-mediated growth method	Supercapacitors	p-type	[72]
Nanoporous copper/copper oxides/reduced graphene oxide (NPC-Cu_2O/CuO/rGO)	Composite structure	Dealloying/microwave—assisted hydrothermal method	Electrochemical	p-p-n type	This work

4. Conclusions

Within this study NPC-Cu_2O/CuO/rGO composite structures were successfully assessed by the dealloying process of $Cu_{48}Zr_{47}Al_5$ amorphous ribbons and the microwave-assisted hydrothermal method. A very important aspect of this hydrothermal method is that both structures, nanoporous metallic copper and graphene oxide, were modified in situ as follows: oxidation of the NPC surface and obtaining p-type Cu_2O/CuO structure, and the reduction of graphene oxide to form n-type rGO. Moreover, during the hydrothermal process, rGO deposition occurred on the copper oxide layer, forming the p-p-n NPC-Cu_2O/CuO/rGO composite structure. The XRD spectra shows that incorporating the

graphene has no effect on the crystalline structure of Cu_2O/CuO and the presence of rGO is slightly observed due to the low amount of graphene in the samples. SEM images clearly evidenced that the surface morphologies of the composite's structures have been influenced by the graphene oxide content and the degree of fullness of the autoclaves. Using electrochemical measurements, the synthesized composite was characterized in terms of internal resistance, showing a series resistance (Rs) of 40 Ω and a charge transfer resistance (Rp) of 250 Ω. Additionally, M-S measurements revealed the n-rGO/p-Cu_2O/CuO electrochemical junction behavior, with calculated carrier densities of 4.2×10^{18} cm^{-3} for rGO, and 7.22×10^{18} cm^{-3} for Cu_2O/CuO, respectively. The NPC-Cu_2O/CuO/rGO composite shows significant potential for supercapacitor applications due to the combined conductivity and active surface area of NPC, along with the high theoretical capacitance of copper oxides. Furthermore, the synergistic effect of rGO prevents particle agglomeration and enhances surface ion diffusion efficiency and mobility, further improving stability and capacity in energy storage.

Author Contributions: Conceptualization, M.N., S.A., C.C. and C.B.; methodology, M.N., S.A., M.M., C.B., C.C. and C.L.; validation C.C. and C.B.; investigation, M.M., I.H., S.A., P.H. and C.O.; writing—original draft preparation, M.N., C.O., C.C., P.H. and C.B.; writing—review and editing, M.N., C.C. and C.B.; visualization, C.C. and C.B.; supervision, C.L., C.C. and C.B. All authors have read and agreed to the published version of the manuscript.

Funding: The authors acknowledge the support of project granted by the Ministry of Research, Innovation and Digitization, CNCS-UEFISCDI, project number PN-IV-P8-8.3-ROMD-2023-0227 within PNCDI IV and partially project number PN 23 27 01 02 INOMAT, 23-27 29N/2023.

Data Availability Statement: The original contributions presented in the study are included in the manuscript.

Conflicts of Interest: The authors declare no conflicts of interest.

References

1. Momeni, M.; Ghayeb, Y.; Menati, M. Fabrication, characterization and photoelectrochemical properties of cuprous oxide-reduced graphene oxide photocatalysts for hydrogen generation. *J. Mater. Sci. Mater. Electron.* **2018**, *29*, 4136–4146. [CrossRef]
2. Norizan, M.N.; Abdullah, N.; Halim, N.A.; Demon, S.Z.; Mohamad, I.S. Heterojunctions of rGO/Metal Oxide Nanocomposites as Promising Gas-Sensing Materials—A Review. *Nanomaterials* **2022**, *12*, 2278. [CrossRef] [PubMed]
3. Singh, J.; Rawat, M. A Brief Review on Synthesis and Characterization of Copper Oxide Nanoparticles and its Applications. *J. Bioelectron. Nanotechnol.* **2016**, *1*, 9. [CrossRef]
4. Sarkar, C.; Dolui, S.K. Synthesis of copper oxide/reduced graphene oxide nanocomposite and its enhanced catalytic activity towards reduction of 4-nitrophenol. *RSC Adv.* **2015**, *5*, 60763–60769. [CrossRef]
5. Jeong, D.; Jo, W.; Jeong, J.; Kim, T.; Han, S.; Son, M.K.; Jung, H. Characterization of Cu_2O/CuO heterostructure photocathode by tailoring CuO thickness for photoelectrochemical water splitting. *RSC Adv.* **2022**, *12*, 2632–2640. [CrossRef]
6. Sun, S.; Zhang, X.; Sun, Y.; Yang, S.; Song, X.; Yang, Z. Facile Water-Assisted Synthesis of Cupric Oxide Nanourchins and Their Application as Nonenzymatic Glucose Biosensor. *ACS Appl. Mater. Interfaces* **2013**, *5*, 4429–4437. [CrossRef]
7. Khayyat, S.A.; Ansari, S.G.; Umar, A. Glucose sensor based on copper oxide nanostructures. *J. Nanosci. Nanotechnol.* **2014**, *14*, 3569–3574. [CrossRef]
8. Ahmad, R.; Tripathy, N.; Hahn, Y.-B.; Umar, A.; Ibrahim, A.A.; Kim, S.H. A robust enzymeless glucose sensor based on CuO nanoseed modified electrodes. *Dalton Trans.* **2015**, *44*, 12488–12492. [CrossRef]
9. Saraf, M.; Natarajan, K.; Mobin, S.M. Non-enzymatic amperometric sensing of glucose by employing sucrose templated microspheres of copper oxide (CuO). *Dalton Trans.* **2016**, *45*, 5833–5840. [CrossRef]
10. Baloach, Q.-U.-A.; Tahira, A.; Mallah, A.B.; Abro, M.I.; Uddin, S.; Willander, M.; Ibupoto, Z.H. A Robust, Enzyme-Free Glucose Sensor Based on Lysine-Assisted CuO Nanostructures. *Sensors* **2016**, *16*, 1878. [CrossRef]
11. Yang, J.; Lin, Q.; Yin, W.; Jiang, T.; Zhao, D.; Jiang, L. A novel nonenzymatic glucose sensor based on functionalized PDDA-graphene/CuO nanocomposites. *Sens. Actuators B Chem.* **2017**, *253*, 1087–1095. [CrossRef]
12. Sahoo, R.K.; Das, A.; Samantaray, K.; Singh, S.K.; Mane, R.S.; Shin, H.-C.; Yun, J.M.; Kim, K.H. Electrochemical glucose sensing characteristics of two-dimensional faceted and non-faceted CuO nanoribbons. *CrystEngComm* **2019**, *21*, 1607–1616. [CrossRef]
13. Liu, M.; Liu, R.; Chen, W. Graphene wrapped Cu_2O nanocubes: Non-enzymatic electrochemical sensors for the detection of glucose and hydrogen peroxide with enhanced stability. *Biosens. Bioelectron.* **2013**, *45*, 206–212. [CrossRef]
14. Zhou, D.-L.; Feng, J.-J.; Cai, L.-Y.; Fang, Q.-X.; Chen, J.-R.; Wang, A.-J. Facile synthesis of monodisperse porous Cu_2O nanospheres on reduced graphene oxide for non-enzymatic amperometric glucose sensing. *Electrochim. Acta* **2014**, *115*, 103–108. [CrossRef]

15. Ding, J.; Sun, W.; Wei, G.; Su, Z. Cuprous oxide microspheres on graphene nanosheets: An enhanced material for non-enzymatic electrochemical detection of H_2O_2 and glucose. *RSC Adv.* **2015**, *5*, 35338–35345. [CrossRef]
16. Wang, Y.; Ji, Z.; Shen, X.; Zhu, G.; Wang, J.; Yue, X. Facile growth of Cu_2O hollow cubes on reduced graphene oxide with remarkable electrocatalytic performance for non-enzymatic glucose detection. *New J. Chem.* **2017**, *41*, 9223–9229. [CrossRef]
17. Yan, X.; Yang, J.; Ma, L.; Tong, X.; Yingyong, W.; Jin, G.; Guo, X. Size-controlled synthesis of Cu_2O nanoparticles on reduced graphene oxide sheets and their application as non-enzymatic glucose sensor materials. *J. Solid State Electrochem.* **2015**, *19*, 3195–3199. [CrossRef]
18. Yazid, S.N.A.M.; Isa, I.M.; Hashim, N. Novel alkaline-reduced cuprous oxide/graphene nanocomposites for non-enzymatic amperometric glucose sensor application. *Mater. Sci. Eng. C* **2016**, *68*, 465–473. [CrossRef]
19. Wang, M.; Song, X.; Song, B.; Liu, J.; Hu, C.; Wei, D.; Wong, C.-P. Precisely quantified catalyst based on in situ growth of Cu_2O nanoparticles on a graphene 3D network for highly sensitive glucose sensor. *Sens. Actuators B Chem.* **2017**, *250*, 333–341. [CrossRef]
20. Cuara, E.; Sierra, U.; Mercado, A.; Barriga-Castro, E.D.; Cortés, A.; Gallardo-Vega, C.; Valle-Orta, M.; Fernández, S. Synthesis of copper oxides-graphene composites for glucose sensing. *Carbon Trends* **2021**, *4*, 100050. [CrossRef]
21. Arnab, H.; Nagesh, S.; Sukumar, B. A Review on Metal Oxide-Graphene Derivative Nano-Composite Thin Film Gas Sensors. In *Multilayer Thin Films*; Sukumar, B., Ed.; IntechOpen: Rijeka, Croatia, 2020; p. Ch. 1.
22. Safaei, M.M.; Abedinzadeh, R.; Khandan, A.; Barbaz-Isfahani, R.; Toghraie, D. Synergistic effect of graphene nanosheets and copper oxide nanoparticles on mechanical and thermal properties of composites: Experimental and simulation investigations. *Mater. Sci. Eng. B* **2023**, *289*, 116248. [CrossRef]
23. Zhu, J.; Yang, D.; Yin, Z.; Yan, Q.; Zhang, H. Graphene and Graphene-Based Materials for Energy Storage Applications. *Small* **2014**, *10*, 3480–3498. [CrossRef] [PubMed]
24. Krsihna, B.V.; Ravi, S.; Prakash, M.D. Recent developments in graphene based field effect transistors. *Mater. Today Proc.* **2021**, *45*, 1524–1528. [CrossRef]
25. Raza, A.; Hassan, J.Z.; Mahmood, A.; Nabgan, W.; Ikram, M. Recent advances in membrane-enabled water desalination by 2D frameworks: Graphene and beyond. *Desalination* **2022**, *531*, 115684. [CrossRef]
26. Bindu, M.; Periyat, P. Graphene and its derivatives for air purification: A mini review. *Results Eng.* **2024**, *21*, 101809. [CrossRef]
27. Velasco, A.; Ryu, Y.K.; Boscá, A.; Ladrón-de-Guevara, A.; Hunt, E.; Zuo, J.; Pedrós, J.; Calle, F.; Martinez, J. Recent trends in graphene supercapacitors: From large area to microsupercapacitors. *Sustain. Energy Fuels* **2021**, *5*, 1235–1254. [CrossRef]
28. Li, S.; Wu, W.; Ma, H.; Zhang, Z.; Gu, Y.; Zhang, J.; Zhang, R. Enhanced molecular sieving performance of thick graphene membranes self-assembled from weakly-oxidized graphene nanosheets. *Appl. Surf. Sci.* **2023**, *615*, 156327. [CrossRef]
29. Liu, J.; Bao, S.; Wang, X. Applications of Graphene-Based Materials in Sensors: A Review. *Micromachines* **2022**, *13*, 184. [CrossRef]
30. Kundu, S.; Karmakar, S.N. Graphene nanopore devices for DNA sequencing: A tight-binding model study. *Phys. B Condens. Matter* **2021**, *623*, 413334. [CrossRef]
31. Liu, X.; Li, Z.; Zhao, W.; Zhao, C.; Wang, Y.; Lin, Z. A facile route to reduced graphene oxide-wrapped octahedral Cu_2O with enhanced photocatalytic and photovoltaic performance. *J. Mater. Chem. A* **2015**, *3*, 19148–19154. [CrossRef]
32. Dubale, A.A.; Su, W.-N.; Tamirat, A.G.; Pan, C.-J.; Aragaw, B.A.; Chen, H.-M.; Chen, C.-H.; Hwang, B.-J. The synergetic effect of graphene on Cu_2O nanowire arrays as a highly efficient hydrogen evolution photocathode in water splitting. *J. Mater. Chem. A* **2014**, *2*, 18383–18397. [CrossRef]
33. Zhang, Z.; Dua, R.; Zhang, L.; Zhu, H.; Zhang, H.; Wang, P. Carbon-Layer-Protected Cuprous Oxide Nanowire Arrays for Efficient Water Reduction. *ACS Nano* **2013**, *7*, 1709–1717. [CrossRef] [PubMed]
34. Zhao, B.; Liu, P.; Zhuang, H.; Jiao, Z.; Fang, T.; Xu, W.; Lu, B.; Jiang, Y. Hierarchical self-assembly of microscale leaf-like CuO on graphene sheets for high-performance electrochemical capacitors. *J. Mater. Chem. A* **2013**, *1*, 367–373. [CrossRef]
35. Chen, J.; Wang, L.; Huang, Y.; Li, Z.; Zhang, H.; Chand Ali, M.; Liu, J.; Chen, X.; Qiu, H. Fabrication of nanoporous graphene/cuprous oxide nanocomposite and its application for chemiluminescence sensing of NADH in human serum and cells. *Sens. Actuators B Chem.* **2019**, *290*, 15–22. [CrossRef]
36. Tian, C.; Zhang, S.; Wang, H.; Chen, C.; Han, Z.; Chen, M.; Zhu, Y.; Cui, R.; Zhang, G. Three-dimensional nanoporous copper and reduced graphene oxide composites as enhanced sensing platform for electrochemical detection of carbendazim. *J. Electroanal. Chem.* **2019**, *847*, 113243. [CrossRef]
37. Wang, L.; Lian, J.; Cui, P.; Xu, Y.; Seo, S.; Lee, J.; Chan, Y.; Lee, H. Dual n-type doped reduced graphene oxide field effect transistors controlled by semiconductor nanocrystals. *Chem. Commun.* **2012**, *48*, 4052. [CrossRef] [PubMed]
38. Haidry, A.A.; Wang, Z.; Fatima, Q.; Zavabeti, A.; Xie, L.; Zhu, H.; Li, Z. Thermally reduced graphene oxide showing n- to p-type electrical response inversion with water adsorption. *Appl. Surf. Sci.* **2020**, *531*, 147285. [CrossRef]
39. Anadkat, D.; Pandya, A.; Jaiswal, A.; Dungani, S.; Sanchela, A. Experimental comparison between graphene and reduced graphene oxide along with significant conversion of rGO from n-to p-type. *J. Mater. Sci. Mater. Electron.* **2024**, *35*, 821. [CrossRef]
40. Bhaumik, A.; Narayan, J. Conversion of p to n-type reduced graphene oxide by laser annealing at room temperature and pressure. *J. Appl. Phys.* **2017**, *121*, 125303. [CrossRef]
41. Wei, L.; Wang, P.; Yang, Y.; Luo, R.; Li, J.; Gu, X.; Zhan, Z.; Dong, Y.; Song, W.; Fan, R. Facile synthesis of nitrogen-doped reduced graphene oxide as an efficient counter electrode for dye-sensitized solar cells. *J. Nanoparticle Res.* **2018**, *20*, 110. [CrossRef]

42. Ma, Z.; Song, P.; Yang, Z.; Wang, Q. Trimethylamine detection of 3D rGO/mesoporous In_2O_3 nanocomposites at room temperature. *Appl. Surf. Sci.* **2019**, *465*, 625–634. [CrossRef]
43. Park, S.Y.; Lee, J.E.; Kim, Y.H.; Kim, J.J.; Shim, Y.-S.; Kim, S.Y.; Lee, M.H.; Jang, H.W. Room temperature humidity sensors based on rGO/MoS2 hybrid composites synthesized by hydrothermal method. *Sens. Actuators B Chem.* **2018**, *258*, 775–782. [CrossRef]
44. Zhang, D.; Liu, J.; Xia, B. Nitrogen Dioxide-Sensing Properties at Room Temperatureof Metal Oxide-Modified Graphene Composite via One-Step Hydrothermal Method. *J. Electron. Mater.* **2016**, *45*, 4324–4330. [CrossRef]
45. May, W. Hydrothermal Oxidation. In *Mobile Alternative Demilitarization Technologies*; Holm, F.W., Ed.; Springer: Dordrecht, The Netherlands, 1997; pp. 155–181.
46. Zhang, F.; Huang, S.; Guo, Q.; Zhang, H.; Li, H.; Wang, Y.; Fu, J.; Wu, X.; Xu, L.; Wang, M. One-step hydrothermal synthesis of Cu_2O/CuO hollow microspheres/reduced graphene oxide hybrid with enhanced sensitivity for non-enzymatic glucose sensing. *Colloids Surf. A Physicochem. Eng. Asp.* **2020**, *602*, 125076. [CrossRef]
47. Zimbovskii, D.S.; Baranov, A.N. Chemical Processes of the Formation of Copper(I) Oxide on Copper Foil under Hydrothermal Conditions. *Inorg. Mater.* **2023**, *59*, 749–756. [CrossRef]
48. Nathan, D.M.G.T.; Boby, S.J.M.; Basu, P.; Mahesh, R.; Harish, S.; Joseph, S.; Sagayaraj, P. One-pot hydrothermal preparation of Cu_2O-CuO/rGO nanocomposites with enhanced electrochemical performance for supercapacitor applications. *Appl. Surf. Sci.* **2018**, *449*, 474–484. [CrossRef]
49. Moghanlou, A.O.; Sadr, M.H.; Bezaatpour, A.; Salimi, F.; Yosefi, M. RGO/Cu_2O-CuO nanocomposite as a visible-light assisted photocatalyst for reduction of organic nitro groups to amines. *Mol. Catal.* **2021**, *516*, 111997. [CrossRef]
50. Thiruppathi, A.R.; van der Zalm, J.; Zeng, L.; Salverda, M.; Wood, P.C.; Chen, A. Effective microwave-hydrothermal reduction of graphene oxide for efficient energy storage. *J. Energy Storage* **2022**, *48*, 103962. [CrossRef]
51. Zhao, C.; Wu, X.; Li, P.; Zhao, C.; Qian, X. Hydrothermal deposition of CuO/rGO/Cu_2O nanocomposite on copper foil for sensitive nonenzymatic voltammetric determination of glucose and hydrogen peroxide. *Microchim. Acta* **2017**, *184*, 2341–2348. [CrossRef]
52. Wang, K.; Dong, X.; Zhao, C.; Qian, X.; Xu, Y. Facile synthesis of Cu_2O/CuO/RGO nanocomposite and its superior cyclability in supercapacitor. *Electrochim. Acta* **2015**, *152*, 433–442. [CrossRef]
53. Lazau, C.; Nicolaescu, M.; Orha, C.; Pop, A.; Căprărescu, S.; Bandas, C. In Situ Deposition of Reduced Graphene Oxide on Ti Foil by a Facile, Microwave-Assisted Hydrothermal Method. *Coatings* **2022**, *12*, 1805. [CrossRef]
54. Vasudevan, D.; Senthilkumar, D.; Surendhiran, S. Performance and Characterization Studies of Reduced Graphene Oxides Aqua Nanofluids for a Pool Boiling Surface. *Int. J. Thermophys.* **2020**, *41*, 74. [CrossRef]
55. Nicolaescu, M.; Hididis, P.; Codrean, C.; Hulka, I.; Vajda, M.; Orha, C.; Bandas, C.; Lazau, C.; Aurel Serban, V. Synthesis of nanoporous copper by dealloying CuZrAl and CuZrAlAg amorphous ribbons in acidic solution. *Mater. Today Proc.* **2023**, *72*, 565–571. [CrossRef]
56. Ursu, D.; Vajda, M.; Miclau, M. Investigation of the p-type dye-sensitized solar cell based on full Cu_2O electrodes. *J. Alloys Compd.* **2019**, *802*, 86–92. [CrossRef]
57. Zhang, C.; Chen, J.; Chen, W.; Liu, J.; Chen, D. Hydrothermal synthesis of Cu_2O/CuO/hierarchical porous N-doped activated carbon with exceptional electrochemical performance. *J. Energy Storage* **2023**, *60*, 106600. [CrossRef]
58. Aqeel, M.; Anjum, S.; Imran, M.; Ikram, M.; Majeed, H.; Naz, M.; Ali, S.; Ahmad, M.A. TiO_2 @ RGO (reduced graphene oxide) doped nanoparticles demonstrated improved photocatalytic activity. *Mater. Res. Express* **2019**, *6*, 086215. [CrossRef]
59. Zhang, Y.; Zhang, N.; Tang, Z.-R.; Xu, Y.-J. Graphene Transforms Wide Band Gap ZnS to a Visible Light Photocatalyst. The New Role of Graphene as a Macromolecular Photosensitizer. *ACS Nano* **2012**, *6*, 9777–9789. [CrossRef]
60. Bai, W.; Wu, M.; Du, X.; Gong, W.; Ding, Y.; Song, C.; Liu, L. Synergistic effect of multiple-phase rGO/CuO/Cu_2O heterostructures for boosting photocatalytic activity and durability. *Appl. Surf. Sci.* **2021**, *544*, 148607. [CrossRef]
61. Heinemann, M.; Eifert, B.; Heiliger, C. Band structure and phase stability of the copper oxides Cu_2O, CuO, and Cu_4O_3. *Phys. Rev. B* **2013**, *87*, 115111. [CrossRef]
62. Choi, K.H.; Ali, A.; Jo, J. Randomly oriented graphene flakes film fabrication from graphite dispersed in N-methyl-pyrrolidone by using electrohydrodynamic atomization technique. *J. Mater. Sci. Mater. Electron.* **2013**, *24*, 4893–4900. [CrossRef]
63. Santhosh, M. µPED based electrode modified with nanocomposite for the detection of proline: An abiotic stress biomarker in plant. *Precis. Agric. Sci. Technol.* **2023**, *5*, 153–161. [CrossRef]
64. Han, J.; Chang, J.; Wei, R.; Ning, X.; Li, J.; Li, Z.; Guo, H.; Yang, Y. Mechanistic investigation on tuning the conductivity type of cuprous oxide (Cu2O) thin films via deposition potential. *Int. J. Hydrog. Energy* **2018**, *43*, 13764–13777. [CrossRef]
65. Gelderman, K.; Lee, L.; Donne, S.W. Flat-Band Potential of a Semiconductor: Using the Mott–Schottky Equation. *J. Chem. Educ.* **2007**, *84*, 685. [CrossRef]
66. Lazau, C.; Poienar, M.; Orha, C.; Ursu, D.; Nicolaescu, M.; Vajda, M.; Bandas, C. Development of a new "n-p" heterojunction based on TiO_2 and $CuMnO_2$ synergy materials. *Mater. Chem. Phys.* **2021**, *272*, 124999. [CrossRef]
67. Zhang, Z.; Wang, P. Optimization of photoelectrochemical water splitting performance on hierarchical TiO_2 nanotube arrays. *Energy Environ. Sci.* **2012**, *5*, 6506. [CrossRef]
68. Moosavifard, S.E.; Mohammadi, A.; Ebrahimnejad Darzi, M.; Kariman, A.; Abdi, M.M.; Karimi, G. A facile strategy to synthesis graphene-wrapped nanoporous copper-cobalt-selenide hollow spheres as an efficient electrode for hybrid supercapacitors. *Chem. Eng. J.* **2021**, *415*, 128662. [CrossRef]

69. Pourbeyram, S.; Abdollahpour, J.; Soltanpour, M. Green synthesis of copper oxide nanoparticles decorated reduced graphene oxide for high sensitive detection of glucose. *Mater. Sci. Eng. C* **2019**, *94*, 850–857. [CrossRef]
70. Saadati pour, M.; Gilak, M.R.; Pedram, M.Z.; Naikoo, G. Enhancement electrochemical properties of supercapacitors using hybrid CuO/Ag/rGO based nanoporous composite as electrode materials. *J. Energy Storage* **2023**, *74*, 109330. [CrossRef]
71. Li, Y.; Zhao, X.; Liu, H.; Li, W.; Wang, X. Synthesis and Morphology Control of Nanoporous Cu_2O/Cu and Their Application as Electrode Materials for Capacitors. *Nanomaterials* **2019**, *9*, 340. [CrossRef]
72. Wongjom, P.; Tuichai, W.; Karaphun, A.; Phrompet, C.; Daengsakul, S.; Pimanpang, S.; Moontragoon, P.; Srepusharawoot, P.; Sriwong, C.; Ruttanapun, C. Characterization and electrochemical properties of CuO–Cu_2O@rGO nanocomposite synthesized by a seed-mediated growth process. *J. Phys. Chem. Solids* **2022**, *163*, 110540. [CrossRef]

Disclaimer/Publisher's Note: The statements, opinions and data contained in all publications are solely those of the individual author(s) and contributor(s) and not of MDPI and/or the editor(s). MDPI and/or the editor(s) disclaim responsibility for any injury to people or property resulting from any ideas, methods, instructions or products referred to in the content.